



Sample size and preparation effects on the tensile ductility of Pd-based metallic glass nanowires

Jun Yi,^{a,*} Wei Hua Wang^b and John J. Lewandowski^a

^aDepartment of Materials Science and Engineering, Case Western Reserve University, 10900 Euclid Avenue, Cleveland, OH 44106, USA

^bInstitute of Physics, Chinese Academy of Sciences, Beijing 100080, People's Republic of China

Received 12 May 2014; revised 30 November 2014; accepted 23 December 2014

Abstract—Glass materials, including metallic glasses (MGs), typically fracture in tension at room temperature in a globally elastic manner. Although homogeneous tensile plasticity and necking of nanoscale MGs have been reported, controversy exists regarding possible contributions from specimen preparation and testing techniques. Here, we show the separate effects of sample size reduction and extrinsic effects on the homogeneous tensile plasticity and necking of Pd₄₀Cu₃₀Ni₁₀P₂₀ glassy wires tested at room temperature. An intrinsic transition from catastrophic shear fracture to plasticity and necking was obtained in this glass when its diameter approached the estimated length scale of the shear-band nucleus size (i.e. 500 nm). A further reduction in the wire diameter to 267 nm produced homogeneous flow and complete ductile necking, with a true fracture strain in excess of 2.0. Our theoretical analysis shows that the plasticity of nanoscale MG wires with diameters smaller than a critical length scale is mediated by shear transformations catalyzed by local shear dilatation, and the predicted critical length scale for the brittle-to-ductile transition of the glassy wires is consistent with our experimental results. Extrinsic effects introduced during sample preparation and/or testing produce entirely different results and are reviewed in the light of previous work.

Published by Elsevier Ltd. on behalf of Acta Materialia Inc.

Keywords: Nanoscale metallic glasses; Catastrophic shear; Complete ductile necking; Shear transformation; Homogeneous plasticity

1. Introduction

Unlike crystalline metals that deform via mobile dislocations and exhibit uniform plasticity prior to necking, glasses without mobile flow defects have no tensile ductility at room temperature (RT) [1–3]. Bulk metallic glasses (MGs) often exhibit compressive plasticity because of their metallic bonding [4], but fracture in tension occurs via catastrophic shear at the elastic limit [5]. Recent reviews have shown that the ductility of crystalline metals can be further enhanced by reducing sample size from bulk to micrometer ranges [6], and nanoscale oxide glass spheres exhibit compressive plasticity even though bulk oxide glasses fail elastically [1]. It can be concluded that such size reductions are effective in enhancing the ductility of many material systems.

Considerable recent work has focused on the mechanical behavior of nanoscale metallic glasses (NMGs). A transition from shear banding to homogeneous plastic deformation in NMGs has been observed by some, but not all, research groups [6]. The existence of an intrinsic size-induced plasticity of MGs remains controversial due to

possible extrinsic effects introduced during sample preparation and/or testing [6,7]. Typical sample preparation techniques including focused ion beam (FIB) milling of samples [8,9], magnetron sputtering of MG films [10–12] and nanomolding of MG nanowires [13,14] have been used to investigate the tensile properties of NMGs. Free volume or gallium ion softening can be introduced by FIB and may also improve the ductility of NMGs [7,13], while heating induced by high-speed gallium ions may promote structural relaxation that reduces ductility [15]. The specimen taper that is typically produced by FIB can also affect the mechanical behavior of NMGs [7,9,11], while the structure of magnetron-sputtered MG films is very different from their bulk counterparts, as pointed out by various authors [16], potentially obscuring any intrinsic size effects. Although nanomolding can be used for fabrication of MG nanowires from bulk counterparts, the exposure of samples to air combined with the compressive stress state and contact of samples with the mold at high temperatures can produce oxidized and/or structurally relaxed samples [17]. Sample manipulation and imaging during in situ testing in a scanning electron microscope or transmission electron microscope can produce heating that can also cause structural relaxation [18] or surface diffusion that promotes diffusive plasticity [1,19]. Most recently, there has been a report of RT homogeneous plasticity obtained in compres-

* Corresponding author. Tel.: +1 2167123623; e-mail: jxy305@gmail.com

sion of micrometer-sized MG pillars fabricated by FIB-machining of sputtered PdSi MG films, along with strain-rate effects on the behavior. This recent work [11] minimized the top rounding of the pillars and ion irradiation effects, while the authors indicated that no extrinsic effects were introduced during testing [11]. The behavior in tension was not investigated in that work [11].

The size effect in MGs has been described by various phenomenological models [9,12,20,21]. In these models, a shear band is treated as a crack driven by the release of elastic energy stored in the sample [9,12,20,21]. However, as pointed out by others [22–24], the behavior of a shear band is very different from that of a crack and these models cannot explain certain experimental data reported in the literature [22]. A more recent phenomenological model utilized the dependence of shear band spacing and shear offset on sample size to depict the size effect obtained during compression studies of magnetron-sputtered and FIB-machined MGs [11]. However, this model alone cannot explain the observed strain-rate effect on the inhomogeneous-to-homogeneous plastic deformation transition. An empirical law describing the ductile-to-brittle transition in a size-rate deformation map was proposed [11] and invoked rate effects on shear band velocity in samples of different sizes. It will be interesting to explore how this empirical law could be applied to tensile deformation given the differences in stress state and test techniques. At elevated temperatures, the brittle-to-ductile transition of MGs has been described by steady-state constitutive flow equations constructed by a free volume model [23] and a shear transformation (ST) model [24,25]. The ST model [25,26] has also been used to describe the transition from inhomogeneous to homogeneous deformation induced by high loading rates in nanoindentation [27].

Here, we demonstrate an intrinsic transition from catastrophic shear fracture to complete ductile necking (i.e. ductile rupture, necking to a point), with evidence of homogeneous flow during tension testing at RT of uniform and smooth Pd₄₀Cu₃₀Ni₂₀P₂₀ glassy wires [28] produced and tension tested without exposure to FIB and/or electron beam. It is shown that wires with diameters smaller than ~500 nm neck during tension tests at RT, while identically sized and smaller MG nanowires previously exposed to either an electron beam or ion beam fail predominantly via catastrophic shear when tested with beam-off conditions. The critical MG nanowire diameter required to produce this brittle-to-ductile transition in the absence of beam exposure is comparable to estimates [26] of the shear band nucleus size for a similar MG. A modified ST theory that incorporates redistribution of the stress and strain fields of STs catalyzed by local shear dilatation is used to explain this transition in deformation behavior of the glassy wires. The effects of various electron- and/or ion-beam exposures on the tensile plasticity of identical nanowires were determined in order to document any extrinsic effects that may arise in sample preparation and/or testing.

2. Experimental methods

2.1. Preparation of MG wires

Pd₄₀Cu₃₀Ni₁₀ ingots were prepared by arc melting Pd, Cu and Ni pieces with purity better than 99.9 wt.% under

a Ti-gettered argon atmosphere in a water-cooled copper hearth. The Pd₄₀Cu₃₀Ni₁₀P₂₀ ingots were prepared by induction heating a Pd₄₀Cu₃₀Ni₁₀ ingot and elemental P crystals with purity better than 99.999 wt.% in a sealed vacuum quartz tube. Because of the evaporation of P during melting, the composition cannot be accurately controlled by melting only once. In an initial trial, 1.2 times the calculated required weight of P was used to make the content of P in the ingot higher than 20 at.%. Then, this ingot and pulverized pieces of Pd₄₀Cu₃₀Ni₁₀ with the amount required to produce the desired final composition (i.e. Pd₄₀Cu₃₀Ni₁₀P₂₀) were sealed in a vacuum quartz tube with B₂O₃ in order to purify the material using a fluxing technique. Pd₄₀Cu₃₀Ni₁₀P₂₀ glassy rods with a diameter of 1 mm were fabricated by a suction-casting method under a Ti-gettered argon atmosphere in a vacuum chamber maintained at 3×10^{-3} Pa. Pd₄₀Cu₃₀Ni₁₀P₂₀ glassy nanowires were then prepared by drawing the glassy rods in their supercooled liquid region. Details of the fabrication method of Pd₄₀Cu₃₀Ni₁₀P₂₀ glassy nanowires can be found elsewhere [28]. The fully amorphous nature of the Pd₄₀Cu₃₀Ni₁₀P₂₀ glassy wire was verified as depicted in previous work [28].

2.2. SEM and ion beam (FIB) exposure of samples

Placement and alignment of the nanowires required some minimal exposure to an electron beam (e.g. 0.17 nA and 5 kV) in the scanning electron microscope prior to tension testing. The initial tension tests did not additionally expose the nanowires to either an electron beam or ion beam until after failure. The current and voltage of the electron beam for SEM imaging of failed MG wires were 1 nA and 20 kV, respectively.

In addition to testing nanowires that had received minimal electron-beam exposure, separate nanowires were studied using an FEI Nova Nanolab 200 to manipulate, image, attach and mill some of the MG wires. The current and voltage of the ion beam for both observation and milling were 10 pA and 30 kV. Pt deposition was used to attach the nanowires to a substrate in some cases, using an electron beam with current and voltage of 4 nA and 15 kV, respectively.

2.3. Tensile testing of MG wires with minimal exposure to electron/ion beam

In order to investigate the intrinsic mechanical behavior of the MG wires, attempts were made to eliminate artifacts during sample preparation, manipulation and testing. The samples used here are uniform and smooth Pd₄₀Cu₃₀Ni₂₀P₂₀ glassy wires fabricated via fast drawing of MG rods in their supercooled liquid region [28]. The wires are rapidly cooled during drawing as they exit the heat source and likely provide an unrelaxed sample. Unfortunately, sample size limitations prevent the use of other conventional characterization techniques (differential scanning calorimetry, dynamic mechanical analysis, etc.). However, the limited heating during preparation of the nanowires should not change the mechanical behavior of the wires, because the critical fictive temperature of the Pd-based glass is higher than its glass transition temperature [29].

Separate MG wires with diameters of 1.48 or 2.5 μm and a 1 cm gauge length were pulled in tension at RT by the method depicted in Fig. 1a. In this case, the wire is fixed

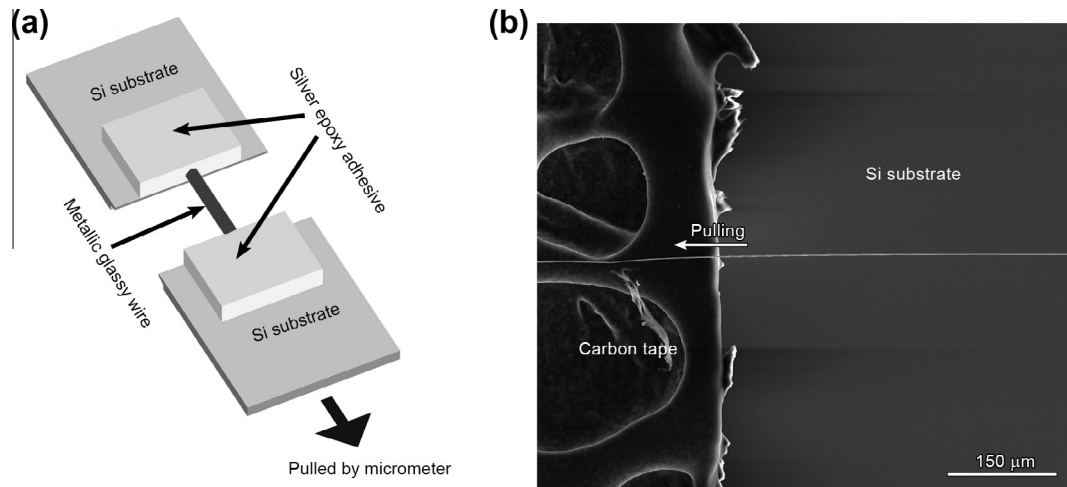


Fig. 1. Tension testing of MG wire. (a) The large-diameter (e.g. 1.48 μm , 2.5 μm) MG wire is fixed to two Si substrates by silver epoxy adhesive. One Si substrate is fixed onto the underlying glass slide, while the other one is driven manually by a micrometer. (b) Tension testing of smaller-diameter wires used a combination of carbon tape and the strong surface adhesion between the Si substrate and nanowire to fix the samples to the Si substrate. In order to ensure good alignment during tension testing, a drop of water was first placed on the Si substrate away from the carbon tape. The smaller-diameter end of the nanowire was then placed on the water drop, followed by the larger-diameter end adhered to the carbon tape, as shown in (b). The Si substrate was then inclined, permitting the water droplet to slide down and away from the end of the nanowire, thereby aligning it with the large-diameter end. The small-diameter end then simply adhered to the Si substrate due to the strong interaction between them [31]. The same underlying glass slide is used during the tension test, performed by using micrometers to pull in the direction indicated by the arrow.

to two Si substrates with silver epoxy adhesive in order to avoid Pt deposition and associated beam exposures. Both Si substrates were on a smooth glass slide and the sample was carefully aligned using fiducial marks on the Si substrates. One Si substrate was fixed to the glass baseplate while the other was manually driven in air at room temperature by a micrometer 20 μm every 3 s (i.e. $\sim 1 \times 10^{-3} \text{ s}^{-1}$ shear strain rate ($\dot{\gamma} = (1 + \nu)\dot{\epsilon}$) [30]). This arrangement provided good alignment of the sample and no exposure to electron/ion beams during tension testing.

Wires of smaller diameter were pulled as shown in Fig. 1b. These tests used a combination of carbon tape and the strong surface adhesion between the Si substrate and nanowire to fix the samples to the Si substrate. These wires all had a larger-diameter end and a nanodiameter end. The larger-diameter end results from the wire drawing process while the diameter of the wire away from this large end is uniform and of nanoscale dimensions with a gauge length of ~ 1 mm. In order to ensure good alignment during tension testing, a drop of water was first placed on the Si substrate away from the carbon tape. The smaller-diameter end of the nanowire was then placed on the water drop, followed by the larger-diameter end adhered to the carbon tape, as shown in Fig. 1b. The Si substrate was then inclined, permitting the water droplet to slide down and away from the end of the nanowire, thereby aligning it with the large-diameter end. The small-diameter end then simply adhered to the Si substrate due to the strong interaction between them [31]. The MG wire was then pulled 2 μm every 3 s (i.e. a shear strain rate of $\sim 1 \times 10^{-3} \text{ s}^{-1}$) in the direction as indicated by the arrow in Fig. 1b at RT. The Si substrates were again present on a glass substrate to ensure additional alignment and the samples tested in this manner received no exposure to either electron or ion beams during tension testing.

3. Results

3.1. Brittle-to-ductile transition

SEM images taken after tension testing are shown in Fig. 2. Wires with diameters of 1.48 and 2.5 μm failed in catastrophic shear as shown in Fig. 2b, similar to the behavior of bulk MGs [5]. However, significant differences in mechanical behavior were obtained in smaller-diameter samples. A diffuse shear band exists in the MG wire with a diameter of 715 nm (Fig. 2c). This sample dislodged from the substrate prior to failure during the tension test. A further diameter reduction to 420 nm produces necking at RT (Fig. 2d). An intrinsic brittle-to-ductile transition is shown in Fig. 2a by quantifying the dependence of the reduction of area $(A_0 - A_f)/A_0$ (where A_f is the cross-sectional area at fracture, and A_0 is the cross-sectional area far away from the failure) on the sample diameter d normalized by the estimated size of the shear band nucleus S_n (i.e. d/S_n , where $S_n = 500$ nm [26] for a similar glass). A transition from catastrophic shear to homogeneous plasticity and necking appears to occur for this material when tested in this manner when the sample diameter approaches S_n (i.e. d/S_n approaches 1.0).

3.2. Towards complete ductile necking (i.e. ductile rupture)

The variation of neck appearance with wire diameter was investigated by testing wires of even smaller diameter. Tension testing of wire with a diameter of 267 nm produced necking to a point (Fig. 3b). This necking does not appear to be preceded by cavitation which is typically observed in ductile engineering materials [32]. In order to further quantify the level of ductility in such samples, Fig. 3a plots the

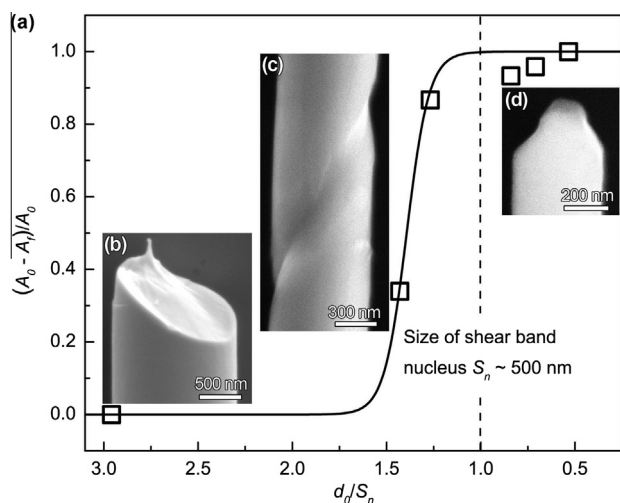


Fig. 2. Transition from catastrophic shear fracture to ductile necking of $\text{Pd}_{40}\text{Cu}_{30}\text{Ni}_{10}\text{P}_{20}$ glassy wires with reduction in sample diameter. (a) Relationship between the reduction of area $(A_0 - A)/A_0$ and diameter of the wires normalized by the shear band nucleus size S_n (i.e. 500 nm) for a similar glass [26]. The reduction of area increases rapidly from 0 to nearly 1 with decreasing diameter of the wires in the range from $d/S_n = 1.6$ to 1.0. (b) Catastrophic shear failure of a MG wire with a diameter of 1.48 or 2.5 μm . (c) Diffuse shear banding of a 715 nm diameter MG wire that dislodged from the Si substrate prior to tensile failure. (d) Necking of a 420 nm diameter MG wire.

true strain ε_T ($\varepsilon_T = \ln(d_0^2/d^2)$) at different normalized distances from the failure sites (i.e. L/d_0) along the axis of the wires, where d_0 is the diameter of wire far away from the failure site, and d is the diameter of wire at the neck. This is not plotted on a linear scale since all samples with diameter $>1.48 \mu\text{m}$ (including bulk samples) are known to fail in catastrophic shear with zero global plasticity.

As shown in Fig. 3a, the 1.48 μm diameter sample that failed in catastrophic shear (Fig. 2b) did not exhibit any change in ε_T along the gauge length. The 2.5 μm diameter sample exhibited the same behavior. However, as the initial wire diameter decreased to 420 and 267 nm, the ε_T increased significantly, and the length of the neck normalized by d_0 increased to 0.54 and 6.49, respectively (Fig. 3a). This demonstrates that the MG wires with smaller diameter prepared and tested in this manner have higher resistance to both fracture and instability to homogeneous plastic deformation [32].

3.3. Extrinsic effects introduced during sample preparation and/or testing

3.3.1. Extrinsic effects on tensile behavior of MG wires

The effects of different sample preparation and testing techniques (Fig. 4) on the mechanical behavior were also studied. To reduce the strong interaction between the Si substrate and nanowires in order to enable manipulation of the nanowires, a Si substrate with trenches was used as shown in Fig. 4a. The nanowire was first adhered to the micromanipulator by deposited Pt, cut by FIB (Fig. 4b), transported to the edge of another Si substrate, adhered to that substrate by Pt deposition and then pulled by the micromanipulator with the beam off (Fig. 4c). In contrast to the plasticity and necking exhibited by the 420 nm diameter wire in Fig. 2d, the MG wire with a diameter of 418 nm

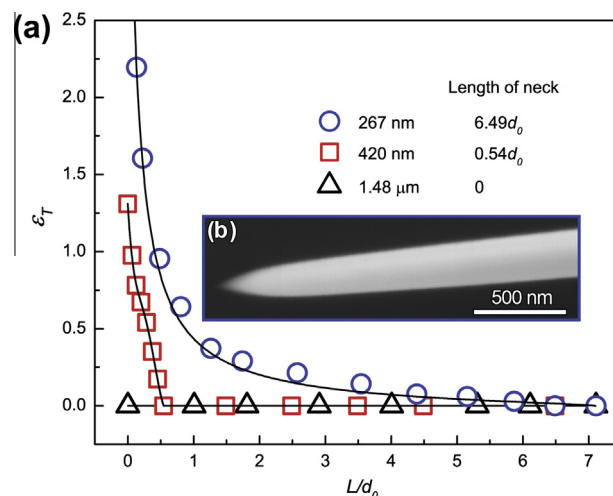


Fig. 3. Towards complete ductile necking of $\text{Pd}_{40}\text{Cu}_{30}\text{Ni}_{10}\text{P}_{20}$ glassy wires. (a) Variation of the true strain with distance along the axis of the wire starting with the failure location. As the starting wire diameter decreases from 1.48 μm (or 2.5 μm) to 267 nm, the length of the neck normalized by d_0 increases from 0 to 6.49. (b) SEM image of a 267 nm diameter MG wire that has necked to a point. The black solid lines in (a) are visual guides. (For interpretation of the references to colour in this figure legend, the reader is referred to the web version of this article.)

tested in this manner failed in catastrophic shear (Fig. 5a). Although a smaller-diameter wire (i.e. 150 nm) tested in this manner produced some local necking (Fig. 5b), the final fracture of this wire was still dominated by shear, unlike the previous results shown in Figs. 2 and 3 that followed the testing method outlined above in Fig. 1. These experimental results appear to be similar to those reported in the literature [9].

The mechanical behavior of smaller-diameter samples ion-milled from our larger-diameter wires was also investigated. A microwire with original diameter of 887 nm was milled (by ion beam) to a sample 358 nm thick as shown in Fig. 6a, and then pulled with the beam off in the manner shown in Fig. 4. Although implantation of gallium ions can introduce free volume or create chemical softening [7,13], the FIB-machined NMG with a thickness of 358 nm only exhibited limited necking with failure in shear (Fig. 6b). Structural relaxation induced by the heating of Pt deposition [33] may contribute to this observation. Experiments to investigate this are underway but beyond the scope of this paper. Figs. 5 and 6 are provided to show that extrinsic effects introduced into our samples produce experimental results similar to those reported in the literature [6] on a range of MGs prepared and/or tested in this manner.

3.3.2. Damage caused by electron beam irradiation

Fig. 7 further shows the self-bending of an originally straight and free-standing MG nanowire caused by irradiation of the electron beam with the same current density and voltage used for Pt deposition. These results indicate that the damage induced by electron beam exposure under these conditions is strong. The lack of bending of FIB-prepared samples reported in the literature [7,9,12], as well as that shown in Fig. 6a, could arise due to the symmetric ion beam exposure used to machine the samples. However, samples that are restricted [8,10] in any manner (e.g.

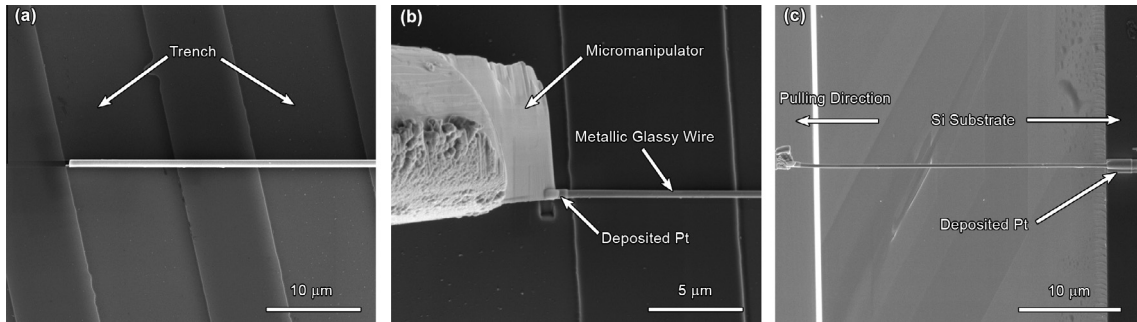


Fig. 4. Procedure for tension testing of MG nanowires using a micromanipulator in a scanning electron microscope. (a) A MG wire positioned for manipulation on a Si substrate with trenches. The width and depth of the trenches are 10 μm and 1 μm , respectively. The distance between trenches is $\sim 10 \mu\text{m}$. (b) Pt deposition used to fix the MG wire to the micromanipulator. The wire was then cut by an ion beam $\sim 20 \mu\text{m}$ away from the Pt deposition. (c) The MG wire is transported to the edge of another Si substrate, adhered to the second Si substrate by deposition of Pt and then pulled in tension by the micromanipulator. The micromanipulator was moved 0.2 μm in $\sim 15 \text{ s}$. The shear strain rate was estimated to be $\sim 1 \times 10^{-3} \text{ s}^{-1}$.

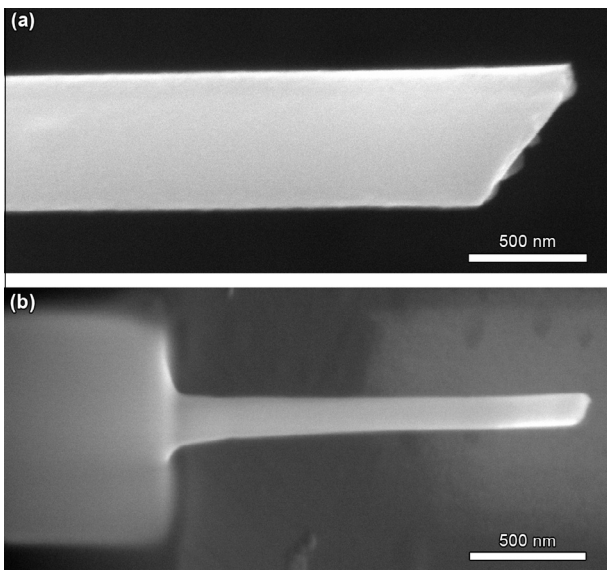


Fig. 5. Fractured $\text{Pd}_{40}\text{Cu}_{30}\text{Ni}_{10}\text{P}_{20}$ glassy wire tested using the method as shown in Fig. 4. (a) Catastrophic shear fracture of $\text{Pd}_{40}\text{Cu}_{30}\text{Ni}_{10}\text{P}_{20}$ glassy wire with a diameter of 418 nm. (b) Tensile failure of a 150 nm diameter MG nanowire. Although there is indication of very local necking, shear dominates the final failure.

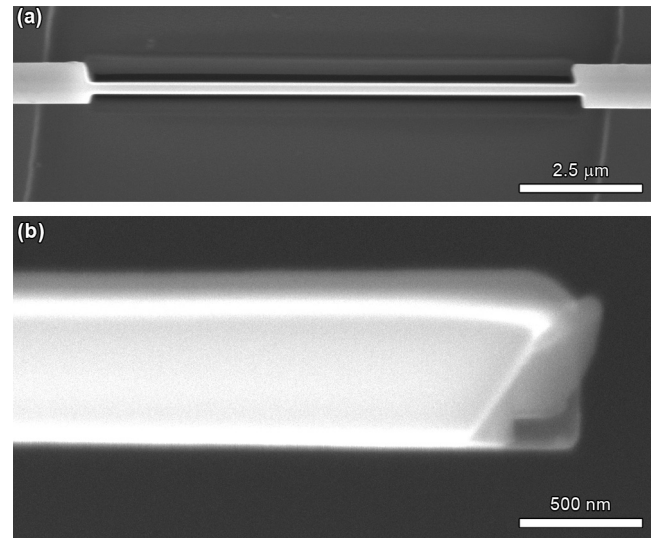


Fig. 6. Effect of ion beam irradiation on tensile fracture of $\text{Pd}_{40}\text{Cu}_{30}\text{Ni}_{10}\text{P}_{20}$ glassy wire. (a) MG nanowire with a reduced thickness of 358 nm milled by a mild ion beam with current and voltage of 10 pA and 30 kV, respectively, from a MG wire with an original diameter of 887 nm. (b) Catastrophic shear failure of the 358 nm NMG in (a) with minimal local necking.

Fig. 6a) are also not permitted to bend, and hence residual stresses may develop as a result. While these effects may not be visible on the machined sample, they will affect the subsequent mechanical behavior.

4. Discussion

The following is an attempt to explain our observations of a size-induced brittle-to-ductile transition based on the original shear transformation theory [34]. Both the local stress and strain field of catalyzed STs (CSTs) are different from isolated STs (ISTs) at low stresses due to the local shear dilatation [26,34,35]. The critical yield stress of CSTs (τ'_0) would be larger than that of ISTs (τ_0) [26,34]. According to the cooperative shear model, the critical yield stress of an ST $\tau_c = \pi\phi_0/4\gamma_c$, where γ_c is the critical shear strain and the total barrier energy density $\phi_0 = (8/\pi^2) \mu\gamma_c^2$ (where

μ is the shear modulus) [36]. Then, $\tau_c = 2\mu\gamma_c/\pi = \sigma_y/\pi$, where σ_y is the yield stress of MGs, i.e. the critical yield stress of an ST is proportional to the yield strength of MGs. Therefore, $\tau'_0/\tau_0 = \sigma_I/\sigma_0$, where σ_I is the strength of MG nanowire, and σ_0 is the bulk strength. Because $\sigma_I^2 - \sigma_0^2 = \Psi/d$ (where Ψ is a material constant based on the Young's modulus and shear band energy density) [22]:

$$\tau'_0 = \tau_0(1 + \Psi/d\sigma_0^2)^{1/2}. \quad (1)$$

The operation of CSTs rearranges the atoms of adjacent transformed volume elements. Such rearrangement releases the strain of the seeding shear transformations [26,34]. The average local shear strain of CST can be written as:

$$\gamma'_0 = \frac{1}{2}\gamma_0, \quad (2)$$

where γ_0 is the local shear strain of an IST. According to ST theory [26,35], the Helmholtz free energy required to operate the CST is:

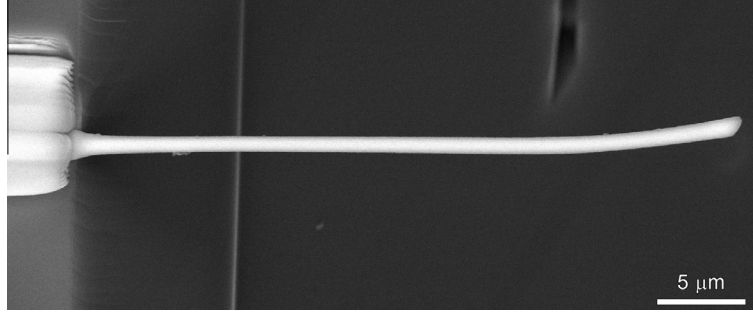


Fig. 7. Self-bending of pristine and originally straight MG nanowire with a diameter of 422 nm caused by electron beam irradiation. The electron beam with 4 nA current and 15 kV voltage is focused in a $1 \times 1 \mu\text{m}^2$ area for 10 s at the right end of an initially straight pristine nanowire. The current and voltage used here is the same as that of electron beam used for Pt deposition. This illustrates that such conditions clearly cause damage and likely affect the subsequent mechanical behavior.

Table 1. List of material constants of $\text{Pd}_{40}\text{Cu}_{30}\text{Ni}_{10}\text{P}_{20}$ glass at RT.

Parameter	Value	Ref.
$\alpha_0 \gamma_0 v_G$	10^{11} s^{-1}	[26,34]
γ_0	0.125	[26,34]
ν	0.394	[36]
β	1	[26,35]
μ	33 GPa	[36]
D	$2.77 \times 10^{-10} \text{ m}$	[39]
σ_0	1.7 GPa	[36]
τ_0/μ	0.03	[26,34]
T_g	593 K	[36]

$$\Delta F'_0 = \left[\frac{7-5\nu}{30(1-\nu)} + \frac{2(1+\nu)}{9(1-\nu)} \beta^2 + \frac{1}{2\gamma'_0} \cdot \frac{\tau'_0}{\mu} \right] \cdot \mu \cdot \gamma_0^2 \cdot \Omega_f, \quad (3)$$

where ν is Poisson's ratio, β is the dilatation factor, which is about unity for MGs [35], T is the temperature, and $\Omega_f = \frac{4}{3}\pi(2.5D)^3$ is the volume of an individual ST (D is the nearest-neighbor distance corresponding to the first peak position in the radial distribution function) [34]. The shear strain rate of a MG sample subjected to a shear stress τ resulting from the superposition of many individual STs is written as:

$$\dot{\gamma} = \alpha_0 \gamma'_0 v_G \cdot \exp\left(-\frac{\Delta F'_0}{kT}\right) \cdot \sinh\left(\frac{\tau \gamma'_0 \Omega_f}{kT}\right), \quad (4)$$

where k is the Boltzmann constant, and α_0 and v_G are pre-exponential coefficients [35] as listed in Table 1. The transition between homogeneous and inhomogeneous deformation can be taken as the critical stress level of $\tau = 0.6\tau'_0$ in Eq. (4) [24]. Incorporating the parameters given in Table 1, Ψ/σ_0^2 , where $\sigma_0 = 1.7 \text{ GPa}$ [36], is estimated to be 670 nm by fitting the experimental data (i.e. dependence of strength on size) of Pd-based glass [37] using the equation $\sigma_f^2 - \sigma_0^2 = \Psi/d$. This leads to the relation between $\dot{\gamma}$ and d/S_n plotted in Fig. 8 that delineates the transition between homogeneous and inhomogeneous deformation. At the present shear strain rate of $\sim 1 \times 10^{-3} \text{ s}^{-1}$, this transition is predicted to occur at $\sim 470 \text{ nm}$, roughly consistent with our experimental results and the calculated shear band nucleus size of 500 nm [26]. Therefore, it appears that the size-induced plasticity of MG nanowires observed here is mediated by CSTs in the shear band nucleus. In the shear band nucleus, STs are catalyzed by the local dilatation in the vicinity of previous shear-transformed sites [26]. During

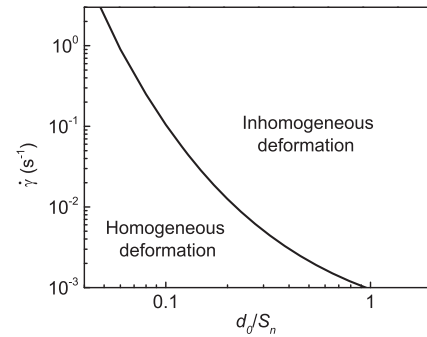


Fig. 8. The transition between homogeneous deformation and inhomogeneous deformation of $\text{Pd}_{40}\text{Cu}_{30}\text{Ni}_{10}\text{P}_{20}$ glass at room temperature, plotting the shear strain rate $\dot{\gamma}$ during tension vs. normalized diameter d/S_n of the MG wire. The transition was calculated using Eq. (4) and the parameters listed in Table 1. This transition at $1 \times 10^{-3} \text{ s}^{-1}$ was estimated at a sample diameter of $0.94S_n$, close to the experimental data shown in Fig. 1 and the size of the shear band nucleus.

the operation of such STs, free volume is redistributed, and the memory of the initial unstressed state is lost [26,35]. Therefore, the material inside the shear band nucleus can undergo plastic deformation. As the sample size approaches the size of the shear band nucleus, shear banding should be preceded by homogeneous plastic deformation since the shear band nucleus cannot percolate to form a shear band as in bulk MGs [38].

5. Concluding remarks

In summary, we show a RT intrinsic transition from catastrophic shear failure to more uniform plasticity and complete ductile necking of a MG when the sample diameter is reduced to below 500 nm when prepared and tested in a manner to avoid extrinsic effects. This sample dimension is of the order of the shear band nucleus size [26] calculated for a similar MG. According to our theoretical analysis, the plasticity of NMGs is mediated by the STs catalyzed by the local dilatation. The prediction of our theoretical analysis on the critical length scale of the brittle-to-ductile transition is consistent with our experimental results. In order to further reveal deformation mechanisms in NMGs, more effort should be made to investigate the behavior of the plasticity carriers (CSTs) in NMGs. Extrinsic effects introduced dur-

ing our sample preparation and/or testing produce entirely different results.

Acknowledgements

The authors appreciate careful review of the manuscript and comments by Ali S. Argon and A. Lindsay Greer. The experimental help of Amir Avishai and Nan Avishai (Swagelok Center for Surface Analysis of Materials) is acknowledged. This work was supported by ARO-W911NF-12-1-0022. W.H.W. appreciates the financial support of the NSF of China under Grant Nos. 51271195 and 51171204.

References

- [1] K. Zheng, C. Wang, Y.Q. Cheng, Y. Yue, X. Han, Z. Zhang, et al., *Nat. Commun.* 1 (2010) 24.
- [2] H. Ni, X. Li, H. Gao, *Appl. Phys. Lett.* 88 (2006) 0431083.
- [3] G. Brambilla, D.N. Payne, *Nano Lett.* 9 (2009) 831.
- [4] Y.H. Liu, G. Wang, R.J. Wang, D.Q. Zhao, M.X. Pan, W.H. Wang, *Science* 315 (2007) 1385.
- [5] T. Mukai, T.G. Nieh, Y. Kawamura, A. Inoue, K. Higashi, *Scr. Mater.* 46 (2002) 43.
- [6] J.R. Greer, J.T.M. De Hosson, *Prog. Mater. Sci.* 56 (2011) 654.
- [7] L. Tian, Z.W. Shan, E. Ma, *Acta Mater.* 61 (2013) 4823.
- [8] H. Guo, P.F. Yan, Y.B. Wang, J. Tan, Z.F. Zhang, M.L. Sui, et al., *Nat. Mater.* 6 (2007) 735.
- [9] D. Jang, J.R. Greer, *Nat. Mater.* 9 (2010) 215.
- [10] Q.S. Deng, Y.Q. Cheng, Y.H. Yue, L. Zhang, Z. Zhang, X.D. Han, et al., *Acta Mater.* 59 (2011) 6511.
- [11] D. Tönnies, R. Maaß, C.A. Volkert, *Adv. Mater.* 26 (2014).
- [12] C.A. Volkert, A. Donohue, F. Spaepen, *J. Appl. Phys.* 103 (2008) 083539.
- [13] D.J. Magagnosc, R. Ehrbar, G. Kumar, M.R. He, J. Schroers, D.S. Gianola, *Sci. Rep.* 3 (2013) 1096.
- [14] D.J. Magagnosc, G. Kumar, J. Schroers, P. Felfer, J.M. Cairney, D.S. Gianola, *Acta Mater.* 74 (2014) 165.
- [15] X. Gu, W. Hao, J. Wang, H. Kou, J. Li, *Rare Met. Mater. Eng.* 39 (2010) 1693.
- [16] Y.H. Liu, T. Fujita, D.P.B. Aji, M. Matsuura, M.W. Chen, *Nat. Commun.* 5 (2014) 3238.
- [17] G. Kumar, H.X. Tang, J. Schroers, *Nature* 457 (2009) 868.
- [18] G.Q. Xie, Q.S. Zhang, D.V. Louzguine-Luzgin, W. Zhang, A. Inoue, *Mater. Trans.* 47 (2006) 1930.
- [19] J.H. Luo, F.F. Wu, J.Y. Huang, J.Q. Wang, S.X. Mao, *Phys. Rev. Lett.* 104 (2010) 215503.
- [20] H. Gao, B. Ji, I.L. Jäger, E. Arzt, P. Fratzl, *Proc. Natl. Acad. Sci.* 100 (2003) 5597.
- [21] Y. Shi, *Appl. Phys. Lett.* 96 (2010) 121909.
- [22] C.C. Wang, J. Ding, Y.Q. Cheng, J.C. Wan, L. Tian, J. Sun, et al., *Acta Mater.* 60 (2012) 5370.
- [23] F. Spaepen, *Acta Metall.* 25 (1977) 407.
- [24] J. Megusar, A.S. Argon, N.J. Grant, *Mater. Sci. Eng.* 38 (1979) 63.
- [25] A.S. Argon, *The Physics of Deformation and Fracture of Polymers*, Cambridge University Press, Cambridge, 2013.
- [26] C.A. Schuh, A.C. Lund, T.G. Nieh, *Acta Mater.* 52 (2004) 5879.
- [27] C.A. Schuh, A.S. Argon, T.G. Nieh, J. Wadsworth, *Philos. Mag.* 83 (2003) 2585.
- [28] J. Yi, X.X. Xia, D.Q. Zhao, M.X. Pan, H.Y. Bai, W.H. Wang, *Adv. Eng. Mater.* 12 (2010) 1117.
- [29] G. Kumar, P. Neibecker, Y.H. Liu, J. Schroers, *Nat. Commun.* 4 (2013) 1536.
- [30] W.F. Hosford, *Mechanical Behavior of Materials*, Cambridge University Press, New York, 2005.
- [31] M.C.P. Wang, B.D. Gates, *Mater. Today* 12 (2009) 34.
- [32] R.W. Hertzberg, *Deformation and Fracture Mechanics of Engineering Materials*, John Wiley, New York, 1996.
- [33] L.A. Gianuzzi, F.A. Stevie, *Introduction to Focused Ion Beams: Instrumentation, Theory, Techniques and Practice*, Springer Verlag, Boston, 2005.
- [34] A.S. Argon, *Acta Metall.* 27 (1979) 47.
- [35] A.S. Argon, L.T. Shi, *Acta Metall.* 31 (1983) 499.
- [36] W.L. Johnson, K. Samwer, *Phys. Rev. Lett.* 95 (2005) 195501.
- [37] B.E. Schuster, Q. Wei, T.C. Hufnagel, K.T. Ramesh, *Acta Mater.* 56 (2008) 5091.
- [38] J.S. Harmon, M.D. Demetriou, W.L. Johnson, K. Samwer, *Phys. Rev. Lett.* 99 (2007) 135502.
- [39] N. Mattern, H. Hermann, S. Roth, J. Sakowski, M.P. Macht, P. Jovari, et al., *Appl. Phys. Lett.* 82 (2003) 2589.